

JGR Atmospheres

RESEARCH ARTICLE

10.1029/2020JD033098

Key Points:

- Conjunctions between Van Allen Probes and FIREBIRD II enable novel estimates of atmospheric electron precipitation
- Estimates of electron precipitation from Van Allen Probes suggest CMIP6 may underestimate atmospheric ionization from 60 to 70 km
- Direct production of NO_x by precipitating electrons during March 2013 using this new method suggest 40% enhancements from 60 to 70 km

Correspondence to:

K. A. Duderstadt,
katharine.duderstadt@unh.edu

Citation:

Duderstadt, K. A., Huang, C.-L., Spence, H. E., Smith, S., Blake, J. B., Crew, A. B., et al. (2021). Estimating the impacts of radiation belt electrons on atmospheric chemistry using FIREBIRD II and Van Allen Probes observations. *Journal of Geophysical Research: Atmospheres*, 126, e2020JD033098. <https://doi.org/10.1029/2020JD033098>

Received 12 MAY 2020

Accepted 22 FEB 2021

Estimating the Impacts of Radiation Belt Electrons on Atmospheric Chemistry Using FIREBIRD II and Van Allen Probes Observations

K. A. Duderstadt¹ , C.-L. Huang¹, H. E. Spence¹ , S. Smith¹, J. B. Blake² , A. B. Crew³ , A. T. Johnson⁴ , D. M. Klumpar⁴, D. R. Marsh⁵ , J. G. Sample⁴ , M. Shumko⁶ , and F. M. Vitt⁵ 

¹The University of New Hampshire, Durham, NH, USA, ²The Aerospace Corporation, Los Angeles, CA, USA, ³Johns Hopkins University Applied Physics Laboratory, Laurel, MD, USA, ⁴Montana State University, Bozeman, MT, USA,

⁵National Center for Atmospheric Research, Boulder, CO, USA, ⁶NASA Goddard Space Flight Center, Greenbelt, MD, USA

Abstract This study considers the impact of electron precipitation from Earth's radiation belts on atmospheric composition using observations from the NASA Van Allen Probes and NSF Focused Investigations of Relativistic Electron Burst Intensity, Range, and Dynamics (FIREBIRD II) CubeSats. Ratios of electron flux between the Van Allen Probes (in near-equatorial orbit in the radiation belts) and FIREBIRD II (in polar low Earth orbit) during spacecraft conjunctions (2015–2017) allow an estimate of precipitation into the atmosphere. Total Radiation Belt Electron Content, calculated from Van Allen Probes RBSP-ECT MagEIS data, identifies a sustained 10-day electron loss event in March 2013 that serves as an initial case study. Atmospheric ionization profiles, calculated by integrating monoenergetic ionization rates across the precipitating electron flux spectrum, provide input to the NCAR Whole Atmosphere Community Climate Model in order to quantify enhancements of atmospheric HO_x and NO_x and subsequent destruction of O_3 in the middle atmosphere. Results suggest that current APEEP parameterizations of radiation belt electrons used in Coupled Model Intercomparison Project may underestimate the duration of events as well as higher energy electron contributions to atmospheric ionization and modeled NO_x concentrations in the mesosphere and upper stratosphere.

Plain Language Summary High-energy particles precipitating into the atmosphere from space affect the chemistry and composition of Earth's atmosphere. While there is significant understanding about the atmospheric impacts of auroral electrons, solar protons, and galactic cosmic rays, the effects of electrons from the near-Earth Van Allen radiation belts remain uncertain. This study helps quantify electrons precipitating into the atmosphere by comparing measurements within the radiation belts from the NASA Van Allen Probes spacecraft to observations from the low-altitude NSF Focused Investigations of Relativistic Electron Burst Intensity, Range, and Dynamics (FIREBIRD II) CubeSats. Global atmospheric model simulations quantify the impact of estimated electron precipitation on the ionization and chemical composition of Earth's atmosphere. Results from an initial case study using this new method suggest that electrons from the radiation belts may produce more atmospheric ionization at lower altitudes and for longer duration than currently recommended estimates, potentially affecting the chemistry of ozone in the middle atmosphere and as a consequence influencing atmospheric heating and dynamics.

1. Introduction

It is widely accepted that protons from impulsive solar events (flares and coronal mass ejections) enhance HO_x ($\text{HO}_x = \text{H} + \text{HO} + \text{HO}_2$) and reactive odd nitrogen ($\text{NO}_x = \text{N} + \text{NO} + \text{NO}_2$) in the middle atmosphere over the polar cap through the dissociation and ionization of N_2 and O_2 (e.g., Funke et al., 2011; Jackman et al., 2008; Randall et al., 2005; Sinnhuber et al., 2012). Low-energy auroral electrons also produce NO_x at high altitudes within the auroral oval. Both short-lived HO_x and longer-lived NO_x participate in the catalytic destruction of ozone (O_3). During polar winter, when downward transport within the isolated polar vortex is strong and photochemistry is limited, NO_x produced in the mesosphere can be transported to the

stratosphere, reducing O₃ levels and modifying the radiative balance, chemistry, and dynamics of the global atmosphere (e.g., Baumgaertner et al., 2011; Duderstadt et al., 2014, 2016; Funke et al., 2011; Rozanov et al., 2005, 2012; Seppälä et al., 2009, 2013).

As consensus grows over the impacts of solar proton events (SPEs) and low energy auroral electrons (<30 keV) on atmospheric HO_x, NO_x, and O₃, research into the contribution of electron precipitation from the Van Allen radiation belts is intensifying (e.g., Andersson, Verronen, Rodger, Clilverd, & Seppälä, 2014; Andersson, Verronen, Rodger, Clilverd, & Wang, 2014; Andersson et al., 2018; Arsenovic et al., 2016; Clilverd et al., 2020; Newnham et al., 2020, 2018; Pettit et al., 2019; Smith-Johnson et al., 2018, 2017). These studies are motivated in part by model simulations that underpredict enhancements of NO_x when only including solar protons, galactic cosmic rays, and auroral electrons (e.g., Andersson et al., 2018; Arsenovic et al., 2016; Randall et al., 2015). The question remains whether ionization from these medium energy electrons (or MEE, typically defined as 30 keV to 1 MeV) can explain these discrepancies (e.g., Callis et al., 1991; Codrescu et al., 1997; Gaines et al., 1995; Sinnhuber et al., 2006, 2012).

The transport, acceleration, and loss of electrons within the Van Allen radiation belts and the relation of these processes to solar storms and geomagnetic disturbances are complex and not yet resolved (e.g., Millan & Thorne, 2007; Reeves et al., 2003; Turner, Morley, et al., 2013). Episodic increases in the precipitation of radiation belt electrons are associated with geomagnetic perturbations driven by solar coronal mass ejections (CMEs) and high-speed solar wind streams (HSSWS) (e.g., Cliver et al., 2006, 2009; Richardson et al., 2000; Rodger et al., 2007; Rozanov et al., 2012; Spence et al., 2013). Electron loss from the radiation belts can be rapid, with examples showing the outer belt emptied within a few days (e.g., Lorentzen et al., 2001; Millan et al., 2007; O'Brien et al., 2004). In addition, a background low flux "drizzle" is constantly present and likely dominates the overall loss rate during quiet times (Kanekal et al., 2001; Millan et al., 2013). While geomagnetic storms have been directly linked with precipitation into the atmosphere, and loss processes such as radial diffusion and magnetopause shadowing are also important, especially during the main storm phase (e.g., Morley et al., 2010; Turner, Angelopoulos, et al., 2013). The competition between sources replenishing electrons in the radiation belts and continued losses, particularly during storm main phase and recovery, makes quantifying these electron loss processes challenging (Reeves et al., 2003; Selesnick, 2006).

The most robust estimates of atmospheric precipitation of radiation belt electrons to date rely on observations from the Medium Energy Proton and Electron Detector (MEPED) instruments on NOAA Polar Orbiting Environmental Satellites (POES) and European Space Agency MetOp satellites (e.g., Matthes et al., 2017; Nesse Tyssøy et al., 2019, 2016; Peck et al., 2015; Pettit et al., 2019; Rodger et al., 2013, 2010; van de Kamp et al., 2018, 2016). The Coupled Model Intercomparison Project (CMIP6) incorporates MEE precipitation using the APEEP model of van de Kamp et al. (2016), a parameterization derived from MEPED data that estimate electron precipitation as a function of the geomagnetic Ap index. Model simulations from Andersson et al. (2018) incorporating CMIP6 APEEP estimates conclude that NO_x enhancements from MEE impact the stratospheric ozone response by a factor of 2. While the APEEP parameterization currently provides the best available radiation belt electron precipitation estimates for decadal-scale atmospheric modeling, uncertainties in the method include how to take into account (1) pitch angle anisotropies, given the narrow field of view of the MEPED telescopes, and (2) estimates of spectral flux at higher energies, given the MEPED integral energy resolution. Nesse Tyssøy et al. (2019) support the argument that the model does not adequately address pitch angle anisotropies. In addition, the authors argue that the APEEP model underestimates electron flux during strong storms, as the parameterization is based on a weak solar cycle and does not take into account the full duration of electron precipitation following storms. We present an alternative method of estimating electron precipitation that addresses uncertainties in MEPED-derived electron precipitation.

This study introduces a novel method of estimating electron precipitation by scaling observations from the Van Allen Probes RBSP-ECT MagEIS instruments (in equatorial orbit at 700 km–6 Re) to observations from the Focused Investigations of Relativistic Electron Burst Intensity, Range, and Dynamics (FIREBIRD II) CubeSats (polar orbiting at 400–600 km). The twin Van Allen Probes provide continuous coverage of electrons trapped within the radiation belts, while FIREBIRD II CubeSats provide sample precipitating electrons from polar low Earth orbit (LEO). We focus on times of moderate geomagnetic activity, excluding periods of strong solar proton events. Both datasets provide higher energy resolution than MEPED

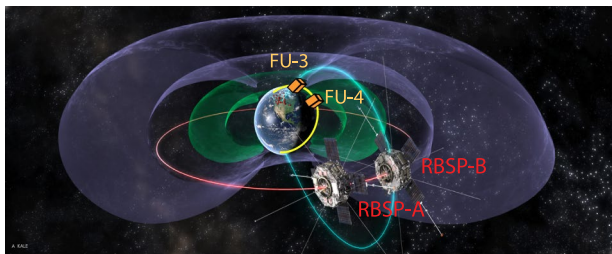


Figure 1. Orbits of the Van Allen Probes (RBSP-A and RBSP-B) (red) and FIREBIRD-II (FU-3 and FU4) (yellow). Representative magnetic field line (blue) observed near the magnetic equator by RBSP-B and at LEO by FU3 during a conjunction. Background image credit A. Kale.

orbit (Crew et al., 2016; Johnson et al., 2020; Shumko et al., 2018; Spence et al., 2012). Each unit carries a FIREBIRD Instrument for Relativistic Electrons (FIRE), measuring high cadence (tens of ms) electron flux across six energy channels from 200 keV to >1 MeV.

Each CubeSat has a surface detector and a collimated detector (see Spence et al., 2012 and Johnson et al., 2020, for instrument details). These silicon solid-state detectors are identical except that the collimated detector has an aluminum collimator above the housing that reduces its angular response and geometric factor. This study uses measurements from the collimated detectors (both FU-3 and FU-4) because the surface detectors did not function as intended for most of the mission and are also more prone to saturation.

The twin NASA Van Allen Probe spacecraft (RBSP-A and RBSP-B) were launched in August 2012. They orbit at an inclination of $\sim 10^\circ$ with altitudes ranging from ~ 700 to $\sim 30,000$ km and pass through both the inner and outer radiation belts. A slight difference in apogee altitudes causes the relative position of these spacecraft to change throughout the mission, allowing for the analysis of temporal and spatial effects (Stratton et al., 2013). The Van Allen Probes Energetic Particle, Composition and Thermal Plasma Suite (RBSP-ECT) instruments are coordinated to measure spatial, temporal, and pitch angle distributions for electrons and ions with energies from tens of electron volt to tens of mega-electron volt (Spence et al., 2013). This study uses data from the Magnetic Electron Ion Spectrometer (MagEIS) that has 25 energy bins (20–4 MeV) and 11 pitch angle bins (8 – 172°) (Blake et al., 2013; Spence et al., 2013).

Figure 1 shows the equatorial orbits of the Van Allen Probes and the low Earth orbits of FIREBIRD II. The broad range of electron energies measured by RBSP-ECT instruments on board the Van Allen Probes provides high resolution differential energy spectra of electrons as a function of L shell and magnetic local time, yielding unprecedented temporal, spatial, and spectral information. However, as a result of the 10° inclination of the spacecraft orbits, the RBSP-ECT instruments do not always sample particles in pitch angles small enough to resolve measurements within the atmospheric loss cone. In contrast, the polar LEO FIREBIRD II CubeSats are designed to observe electrons within the loss cone, allowing the direct evaluation of precipitating electron flux. However, FIREBIRD II is limited by sparse temporal and spatial coverage, as the CubeSats pass quickly through geomagnetic latitudes corresponding to the radiation belts. The size of the loss cone depends on L shell, altitude, and the magnetic field strength, with the loss cone being roughly $\sim 4^\circ$ at the equatorial location of the Van Allen Probes and $\sim 60^\circ$ as the FIREBIRD-II CubeSats pass through outer radiation belt L shells.

Table 1 compares selected past and present satellite instruments that allow estimates of energetic electron precipitation. The twin Van Allen Probes are ideal for providing global coverage of pitch angle resolved, high-resolution observations within the radiation belts. The FIREBIRD II observation sample precipitating electrons with an energy range and resolution are ideal for assessing the production of NO_x in the mesosphere and upper stratosphere, and their polar orbit passes through L-shells associated with the radiation belts. In contrast, while the UARS PEM observations are also of high resolution in the energies of interest, the spacecraft orbit at an inclination of 57° , limiting measurements to electron precipitation from lower L shells ($L < 4$) and not capturing the full extent of the outer radiation belt. SAMPEX PET observations were

instruments and are more sensitive during periods of low flux, conceivably enabling better estimates of the electron precipitation during storm recovery and quiet times and resolving higher energies responsible for atmosphere ionization at lower altitudes. As an initial case study, this paper applies the new method to a 10-day sustained electron loss event observed in the radiation belts during March 2013. Results suggest that CMIP6 particle precipitation may underestimate ionization rates in the mesosphere and upper stratosphere, with potentially significant impacts on the production and background levels of NO_x .

2. Measurements, Model, and Methods

2.1. Measurements

The FIREBIRD II CubeSats, identified as Flight Unit 3 (FU-3) and Flight Unit 4 (FU-4), were launched in January 2015 in polar low Earth orbit (Crew et al., 2016; Johnson et al., 2020; Shumko et al., 2018; Spence et al., 2012). Each unit carries a FIREBIRD Instrument for Relativistic Electrons (FIRE), measuring high cadence (tens of ms) electron flux across six energy channels from 200 keV to >1 MeV.

Each CubeSat has a surface detector and a collimated detector (see Spence et al., 2012 and Johnson et al., 2020, for instrument details). These silicon solid-state detectors are identical except that the collimated detector has an aluminum collimator above the housing that reduces its angular response and geometric factor. This study uses measurements from the collimated detectors (both FU-3 and FU-4) because the surface detectors did not function as intended for most of the mission and are also more prone to saturation.

The twin NASA Van Allen Probe spacecraft (RBSP-A and RBSP-B) were launched in August 2012. They orbit at an inclination of $\sim 10^\circ$ with altitudes ranging from ~ 700 to $\sim 30,000$ km and pass through both the inner and outer radiation belts. A slight difference in apogee altitudes causes the relative position of these spacecraft to change throughout the mission, allowing for the analysis of temporal and spatial effects (Stratton et al., 2013). The Van Allen Probes Energetic Particle, Composition and Thermal Plasma Suite (RBSP-ECT) instruments are coordinated to measure spatial, temporal, and pitch angle distributions for electrons and ions with energies from tens of electron volt to tens of mega-electron volt (Spence et al., 2013). This study uses data from the Magnetic Electron Ion Spectrometer (MagEIS) that has 25 energy bins (20–4 MeV) and 11 pitch angle bins (8 – 172°) (Blake et al., 2013; Spence et al., 2013).

Figure 1 shows the equatorial orbits of the Van Allen Probes and the low Earth orbits of FIREBIRD II. The broad range of electron energies measured by RBSP-ECT instruments on board the Van Allen Probes provides high resolution differential energy spectra of electrons as a function of L shell and magnetic local time, yielding unprecedented temporal, spatial, and spectral information. However, as a result of the 10° inclination of the spacecraft orbits, the RBSP-ECT instruments do not always sample particles in pitch angles small enough to resolve measurements within the atmospheric loss cone. In contrast, the polar LEO FIREBIRD II CubeSats are designed to observe electrons within the loss cone, allowing the direct evaluation of precipitating electron flux. However, FIREBIRD II is limited by sparse temporal and spatial coverage, as the CubeSats pass quickly through geomagnetic latitudes corresponding to the radiation belts. The size of the loss cone depends on L shell, altitude, and the magnetic field strength, with the loss cone being roughly $\sim 4^\circ$ at the equatorial location of the Van Allen Probes and $\sim 60^\circ$ as the FIREBIRD-II CubeSats pass through outer radiation belt L shells.

Table 1 compares selected past and present satellite instruments that allow estimates of energetic electron precipitation. The twin Van Allen Probes are ideal for providing global coverage of pitch angle resolved, high-resolution observations within the radiation belts. The FIREBIRD II observation sample precipitating electrons with an energy range and resolution are ideal for assessing the production of NO_x in the mesosphere and upper stratosphere, and their polar orbit passes through L-shells associated with the radiation belts. In contrast, while the UARS PEM observations are also of high resolution in the energies of interest, the spacecraft orbit at an inclination of 57° , limiting measurements to electron precipitation from lower L shells ($L < 4$) and not capturing the full extent of the outer radiation belt. SAMPEX PET observations were

Table 1
Comparison of Observations of Electron Particle Flux

	UARS (PEM)	SAMPEX (PET)	POES (MEPED)	FIREBIRD II ^a	Van Allen Probes (ECT/ MagEIS)
Altitude	600 km	520–670 km	800–870 km	400–600 km	700 km to ~6 Earth radii
Inclination	57°	82°	98.7°	99.1 °	10°
Energies	30 keV to 4 MeV 32 energy channels	150 keV ^b to 100 s MeV $E > 0.6$ MeV $1.5 < E < 6$ MeV $2.5 < E < 14$ MeV	$E1 > 50$ keV $E2 > 100$ keV $E3 > 300$ keV $P6 > 1$ MeV	265 keV 354 keV 481 keV 663 keV 913 keV >1 MeV	20 keV to 4 MeV 25 energy bins
Challenges	Low L shells	High energies	Proton contamination & noise floor	Sparse & uncertain orientation	Equatorial “near” loss cone

Note. References include UARS—Winningham et al. (1993); SAMPEX—Selesnick et al. (2003); MEPED—Nesse Tyssøy et al., (2016); FIREBIRD II—Crew et al., (2016); Van Allen Probes—Spence et al., (2013).

^aFIREBIRD energy channels vary between campaigns and units. Energies are from FU-3 during multiple campaigns. ^bSAMPEX has 3 years of data from a >150 keV channel but most of the mission observed only higher energies.

at a favorable inclination and provided 3 years of data within an energy channel of >150 keV, but for most of the mission, the instruments sampled energies are too high to adequately predict ionization in the middle atmosphere (Selesnick et al., 2003; Tu et al., 2010). NOAA POES and MetOp MEPED observations have both the inclination and energy range for studying atmospheric impacts and provide broad temporal and spatial coverage with multiple satellites. However, the MEPED integral energy resolution is low, there are significant challenges removing the effects of proton contamination (Nesse Tyssøy et al., 2019; Peck et al., 2014; van de Kamp et al., 2016), and the narrow field of view (30°) and geometric factors of the telescopes result in a high noise floor (Lam et al., 2010; Peck et al., 2015; Rodger et al., 2010; Yando et al., 2011). As alluded to earlier, there are also uncertainties associated with anisotropic pitch angle distributions. Specifically, the geometry and orientation of the MEPED telescopes is such that the 0° detector will underestimate and the 90° detector will overestimate the flux of precipitating electrons (Nesse Tyssøy et al., 2016, 2019; Rodger et al., 2013).

Unique benefits of using FIREBIRD II observations to quantify radiation belt electron precipitation include:

1. High differential energy resolution in an ideal range for studying the direct production of NO_x in the middle atmosphere
2. Instrument geometry providing a field of view of ~60° and geometric factors 600 times greater than POES MEPED (Johnson et al., 2020)
3. Low altitude polar orbit (400–600 km), where the majority of observed electrons are within the drift lost cone and are eventually lost to the atmosphere

However, the FIREBIRD II dataset is limited in spatial and temporal coverage as a result of orbit, data storage, and download limits. In addition, while the CubeSats (and detectors) were designed to use passive magnetic attitude control to point nominally away from the Earth in the Northern Hemisphere, they are still prone to oscillation (wobble) and their precise orientation is unknown (Crew et al., 2016; Johnson et al., 2020). As a consequence, the detectors may sample quasi-trapped (drift loss cone) electrons in addition to directly precipitating electrons (bounce loss cone). Finally, observations are limited to electron energies above ~200 keV and do not measure lower energy electrons responsible for the majority of NO_x production above ~80 km.

2.2. Model

Van Allen Probes observations suggest a broad magnetic footprint of electron precipitation extending to sub-auroral latitudes (50° to 80°). These energetic electrons penetrate atmospheric depths ranging from 90 km (~30 keV) to below 50 km (>2 MeV). The wide horizontal and deep vertical ranges of atmospheric

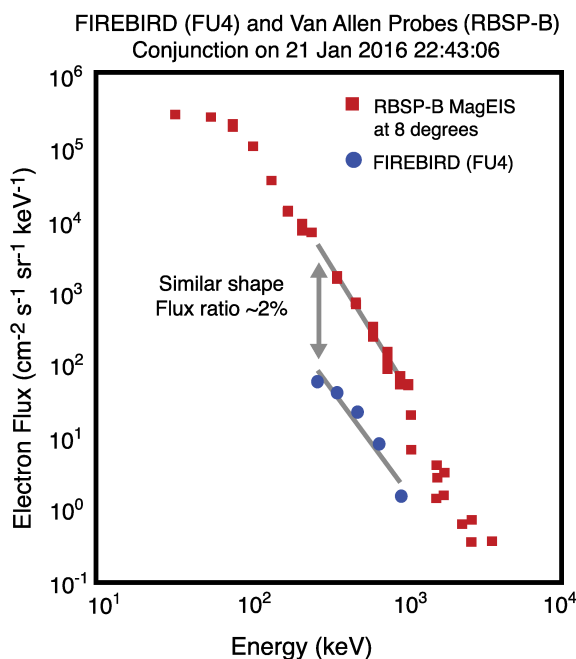


Figure 2. Electron flux observations during a conjunction between RBSP-B and FU4 on 21 January 2016 at 22:43:06.

influence warrant the use of a whole atmosphere, three-dimensional global climate model to study the atmospheric impacts of radiation belt electrons. This project quantifies the effects of atmospheric ionization from radiation belt electrons using the NCAR Whole Atmosphere Community Climate Model (CESM2-WACCM6), a high top model capable of calculating the effects of ionization on atmospheric chemistry and the contribution of the upper atmospheric to climate (Gettelman et al., 2019).

WACCM6 provides 1° horizontal resolution and extends to ~140 km, resolving upper atmospheric processes crucial for accurately modeling the chemical-radiative-dynamic coupling necessary for studying stratospheric ozone and its climate effects (e.g., Charlton-Perez et al., 2013; Garcia et al., 2007; Gettelman et al., 2019; Marsh et al., 2013, 2007). This work takes advantage of the most recent updates to the WACCM6 model, including a new D-region ion chemistry scheme (Verronen et al., 2016). This model chemistry applies 30-min time steps. Simulations in this study use the “specified dynamics” configuration, where meteorological fields below 60 km are nudged using NASA Modern-Era Retrospective analysis for Research and Applications Version 2 (MERRA-2) reanalysis (Gelaro et al., 2017). WACCM6 relies on the CMIP6 solar forcing as described in Matthes et al. (2017). For solar protons, daily averaged ionization rates are calculated based on particle flux measured by GOES and the parameterization of Jackman et al. (1980). Ionization from galactic cosmic rays is determined using modulation potential. Ionization from auroral electrons is based on the parameterization scheme of Roble and Ridley (1987) as described in Marsh et al. (2007). The low energy auroral electrons are primarily significant above 90 km, altitudes higher than the region of this study.

2.3. Methods

2.3.1. Estimating Electron Precipitation From Van Allen Probes Observation

We use the following procedure to estimate ratios of electrons trapped within the radiation belts to electron precipitation into the atmosphere, with an example provided in Figure 2:

1. Determine conjunctions between Van Allen Probes and FIREBIRD II satellites, when satellite orbits are within one L shell and 1h magnetic local time (MLT) and when both RBSP-ECT and high-resolution FIREBIRD II data are available
2. Compare the electron energy spectra of RBSP-ECT and FIREBIRD II at conjunctions
3. Calculate the flux ratio between the loss cone and equatorial plane as a function of electron energy

$$\text{Flux ratio} = \frac{\text{Electron flux in loss cone}}{\text{Electron flux at equator near loss cone}} \%$$

The scaled differential electron flux measured near the loss cone by RBSP-ECT is used to create maps of electron flux at the top of the atmosphere. These precipitation maps allow us to calculate atmospheric ionization input files (ion pair production rates) for WACCM.

This work uses statistics (50th, 75th, and 100th percentiles) of ratios from 35 satellite conjunctions (~50,000 timesteps) during the first 2 years of overlap between FIREBIRD II and the Van Allen Probes missions (2015–2017). These conjunctions were identified among all RBSP and FIREBIRD II spacecraft. We focus on electron flux at geomagnetic latitudes corresponding to L shells three through seven, the region most likely associated with precipitation from the outer radiation belt, and do not consider conjunctions over the South Atlantic Anomaly.

4–14 March 2013 Electron Long Decay Event

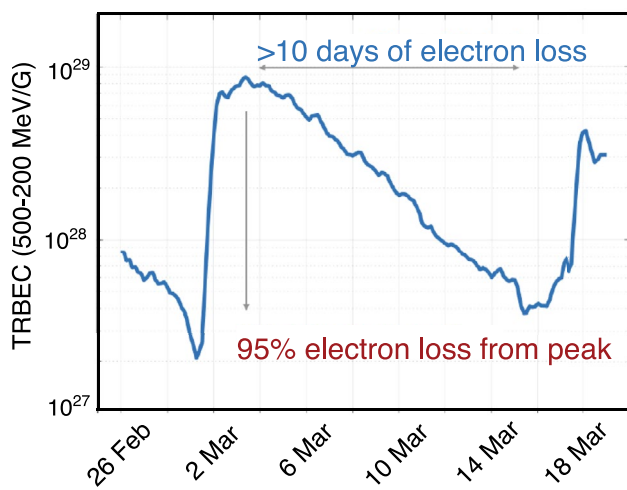


Figure 3. Electron loss event observed by the Van Allen Probes during 4–14 March 2013. Total Radiation Belt Electron Content (TRBEC) is calculated by integrating phase space density determined from Van Allen Probes MagEIS data.

A sustained electron loss event observed by the Van Allen Probes from 4 to 14 March 2013 serves as an initial test case for this new method (Figure 3). This event was identified from Total Radiation Belt Electron Content (TRBEC), calculated by integrating the phase space density data from Van Allen Probes MagEIS over adiabatic invariants (e.g., Forsyth et al., 2016; Hartley & Denton, 2014; Murphy et al., 2018). This event is associated with a HSSWS originating from a coronal hole that began on 28 February 2013 with a duration of 6 days (Gerontidou et al., 2018). The geomagnetic indices Dst and Ap for this time period are presented in Figure 4. TRBEC calculations suggest a 95% loss of electrons over a 10-day period occurring during the recovery phase following the moderate storm. Although FIREBIRD II observations were not yet available during this time, the event provides an excellent case study given the length of decay between storms. The event also occurred early in the Van Allen Probes mission and is highlighted in several publications, including Baker et al. (2014), Li et al. (2014), Reeves et al. (2016), and Ripoll et al. (2016). Results of these studies show evidence of electron loss in addition to radial diffusion within the radiation belts, suggesting pitch angle scattering might be leading to significant electron precipitation to the atmosphere during this time.

We scale the energy-dependent electron flux observed by the Van Allen Probes RBSP-A MagEIS instruments within the smallest pitch angle bin ($<8^\circ$) during this event according to results from the statistical study of flux ratios during satellite conjunctions. We then compare enhancements of nitric oxide (NO) during WACCM simulations with satellite observation using the Odin submillimeter radiometer instrument (Odin/SMR) (Pérot et al., 2014) as well as the Solar Occultation for Ice Experiment (SOFIE) instrument on board the Aeronomy of Ice in the Mesosphere (AIM) (Gordley et al., 2009). The objective of these comparisons is to assess how much of the electron depletion observed within the outer radiation belt can be attributed to atmospheric precipitation.

2.3.2. Calculating Atmospheric Ionization Profiles

Vertical profiles of energy deposition and ion pair production rates are calculated by integrating monoenergetic ionization rates across the differential spectrum of precipitating electrons as outlined in Fang et al. (2010). This method uses coefficients of polynomial fits to first-principle particle transport model results to calculate energy dissipation functions and ionization, integrating across an incident differential energy spectrum to obtain total ionization profiles. The ionization rates calculated using the Fang et al. (2010)

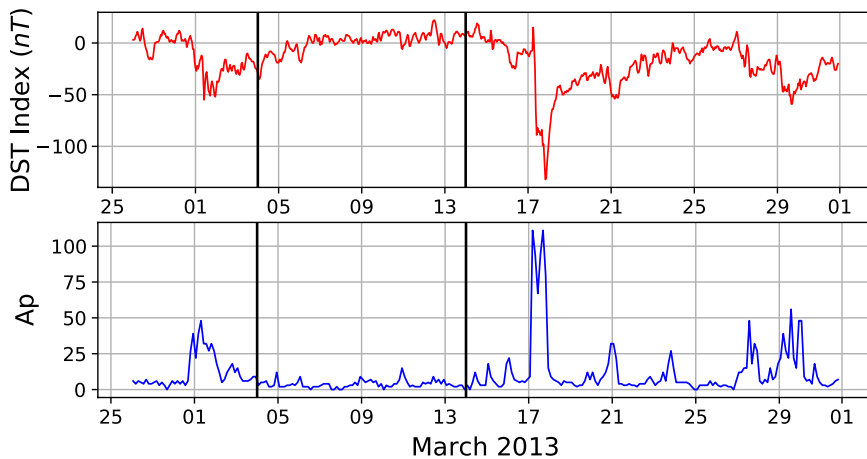


Figure 4. Dst and Ap indices during late February through March 2013 (downloaded from the Kyoto database <http://wdc.kugi.kyoto-u.ac.jp>, August 2020). Vertical black lines indicate the start and end of the 4–14 March 2013 electron loss event considered in this study.

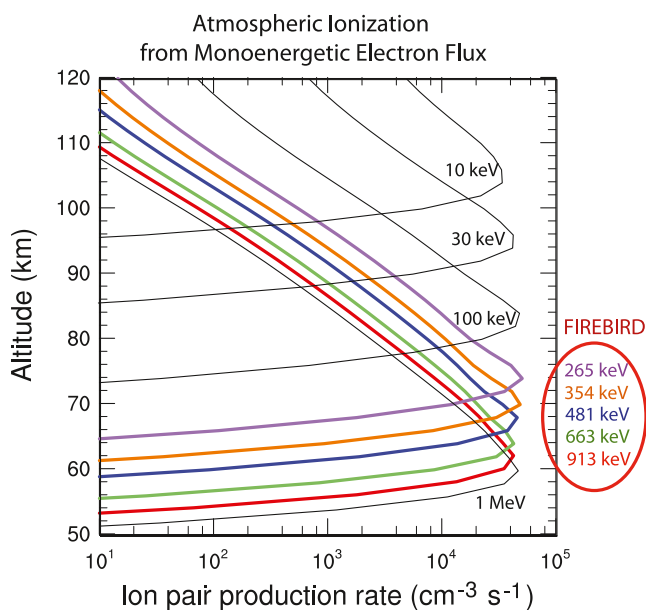


Figure 5. Ionization profiles for monoenergetic electron flux (total incident energy of $1 \text{ erg cm}^{-2} \text{ s}^{-1}$) using the Fang et al. (2010) parameterization. Calculations are based on density and temperature from the MSIS-E-90 atmospheric model on 4 March 2013 at 60°N 0°E . Examples using FIREBIRD-II energies from FU-3 are highlighted in color.

the majority of times. The largest precipitation flux ratios (100th percentile) range from $\sim 7\%$ at 300 keV to $\sim 90\%$ near 900 keV, with many conjunctions between the 75th and 100th percentiles suggesting stronger precipitation events. While the median flux ratio has minimal energy dependence, there are many instances of preferential precipitation at higher energies. There are also conjunctions where the ratio peaks at mid-range energies. It is possible that this energy dependence could be a statistical artifact because of lower particle counts at higher energies or associated with the uncertain orientation of the FIREBIRD II detectors (Johnson et al., 2020). The lower energy channels can also exhibit saturation that might contribute to higher ratios at higher energies. However, behaviors within the radiation belts such as wave-particle interactions can also scatter and precipitate electrons at preferential energies. C.-L. Huang is currently leading a study to assess this energy dependence along with the potential relationship of flux ratios with L shell, magnetospheric activity, and wave-particle interactions. This study will consider the full period of overlap between the Van Allen Probes and FIREBIRD-II missions (2015–2019). Specifically, it will focus on FIREBIRD II high-resolution data downloads targeted during conjunctions with Van Allen Probes beginning in August 2018.

Figure 7 presents observed Van Allen Probes (RBSP-A) daily average flux values for the lowest pitch angle bin ($<8^\circ$) centered on L shells 4, 4.5, 5, and 5.5 ($+/ - 0.25$) throughout the March 2013 electron loss event in energies ranging from 57 keV to 1.7 MeV. Reeves et al. (2016) and Ripoll et al. (2016) provide detailed descriptions of the unique energy dependence of electrons during this time period. For our modeling study, we exponentially extrapolate flux values below 57 keV and above 1.7 MeV, noting that this exponential assumption may underestimate flux values at lower energies as suggested by the spectral fits of MEPED observations by Peck et al. (2015) and the combined RBSP-ECT dataset of Boyd et al. (2019). The Van Allen Probes flux values are multiplied by the flux ratios shown in Figure 6 to estimate electron precipitation at the top of the atmosphere. (Note that the flux ratios for the lowest FIREBIRD II energy channels are used for energies below 200 keV and the highest FIREBIRD II energy channels for energies greater than 1 MeV.)

These scaled electron fluxes are used to create precipitation maps across L shells three through seven ($\sim 55^\circ - 68^\circ$ magnetic latitudes assuming a centered dipole magnetic field). We extend the flux values determined from L shells 3.5 to 5.5 to L shells three through seven, acknowledging the potential for overestimating

parameterization compare well with the CRAC:EPII calculations by Artamanov et al. (2016, 2017), with biases under 35%–40%. The unique ability of FIREBIRD II data to study ionization at middle atmospheric altitudes is shown in Figure 5, with peak ionization ranging from ~ 55 to 75 km at FIREBIRD II energies.

This WACCM study also uses the recently developed D-region ion chemistry scheme (WACCM-D) to calculate HO_x and NO_x production (Verronen et al., 2016), a chemical mechanism that includes 307 reactions of 20 positive ions and 21 negative ions. The primary difference from prior (CESM1-WACCM4) chemistry is that instead of assuming a parameterized production of NO_x and HO_x as described in Jackman et al. (1980, 2009), this new scheme more realistically simulates the full chemical chain from the initial ionization of N_2 and O_2 , through cluster ion reactions, to the ultimate production of NO_x and HO_x . Andersson et al. (2016) conclude that WACCM-D shows closer agreement with observations, producing 25%–50% less OH and 30%–130% more NO_x at 70–85 km.

3. Results

3.1. Electron Precipitation and Atmospheric Ionization Rates

The energy dependent flux ratios for precipitating (FIREBIRD II) and trapped (Van Allen Probes) electrons during 35 conjunctions are given in Figure 6. The median precipitation rate (50th percentile) across all energies is $\sim 1\%$, with 75% of the ratios below 2%–3%. These ratios represent

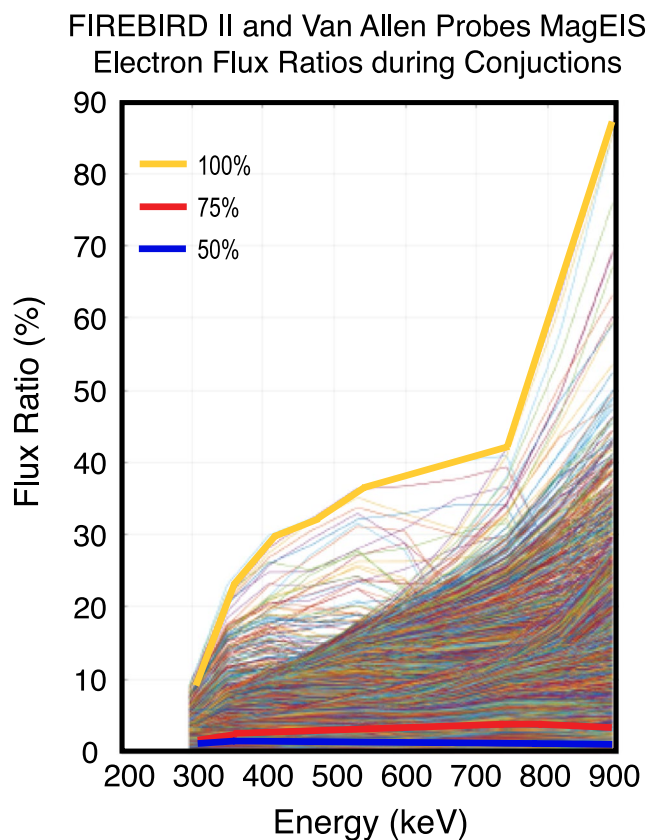


Figure 6. The flux ratios (given in %) between FIREBIRD-II and Van Allen Probes MagEIS electron flux as a function of energy for the 35 conjunctions (50,000 timesteps). Flux ratios associated with 50th (blue), 75th (red), and 100th (yellow) percentiles are overlaid onto plot.

precipitation, as electron flux is not evenly distributed and generally peaks between L shells 4.5 and 5.5 (e.g., Rodger et al., 2010; Verronen et al., 2020). No variability in precipitation is assumed across magnetic local time (longitude). This is an adequate approximation, especially for the study of longer-lived NO_x and O_3 , given the rapid zonal mixing in the atmosphere at these high altitudes (Verronen et al., 2020). Figure 8 shows ionization profiles at an L shell of five using flux ratios representing the 50th (median), 75th, and 100th percentiles from the conjunction study. Figure 9 provides an example of atmospheric ionization rates driving our median flux ratio WACCM simulations. The vertical profile of the atmospheric ionization rates event at 65°N latitude and 0° longitude confirm that energetic electron precipitation from the radiation belts dominates ionization in early March compared with solar protons (noting that this simulation does not include radiation belt precipitation after 14 March). Galactic cosmic rays primarily impact altitudes below 25 km and are therefore not significant to our analysis. Figure 9 also depicts a polar view of the Northern Hemisphere, showing the latitudinal extent of peak ionization on 4 March at the altitude of 70 km.

3.2. WACCM Simulations for March 2013

Figure 10 shows results from WACCM simulations for the March 2013 electron loss event, where radiation belt electron precipitation is included from 26 February through 14 March. Plots focus on a location directly impacted by electron precipitation (65°N latitude and 0° longitude) and exhibit some variability from background atmospheric dynamics. Enhancements of HO_x for the median (50th percentile) ratios are small and limited to higher altitudes (~30% at 70 km). However, the highest flux ratios (100th percentile) result in HO_x enhancement several times larger throughout the mesosphere (~250% at 70 km). Similarly, NO_x enhancements at 70 km are ~40% for the median case but reach up to 30 times background levels for the highest flux ratios. The localized O_3 reductions

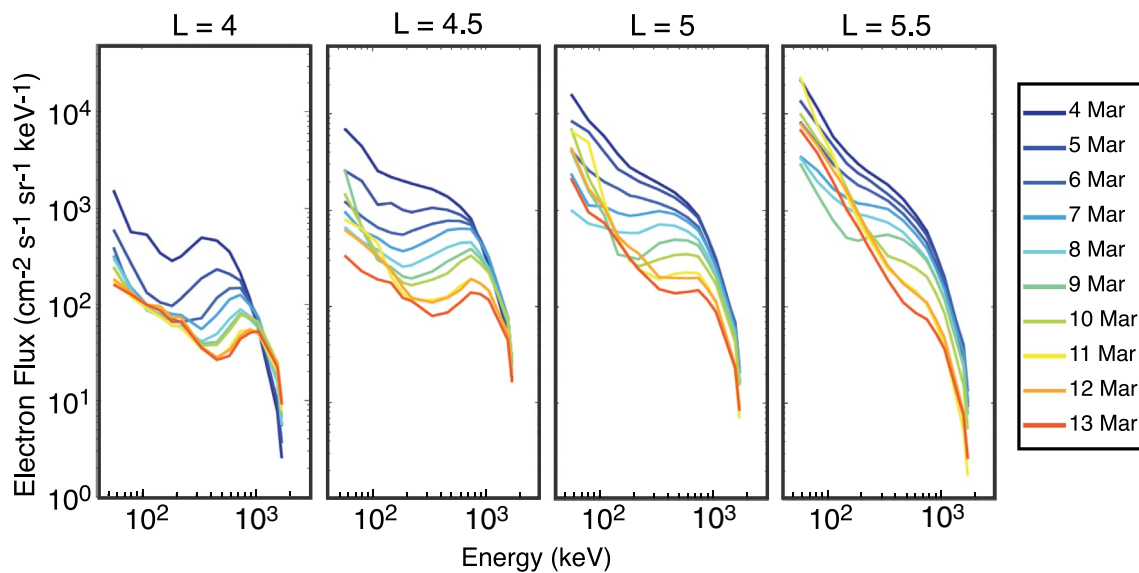


Figure 7. Daily averaged differential electron flux observed by the Van Allen Probes (RBSP-A) ECT-MagEIS instrument for the 4–14 March 2013 event for pitch angles <8° at several L-shells. These values are multiplied by the energy dependent flux ratios presented in Figure 6 to estimate electron precipitation to the atmosphere.

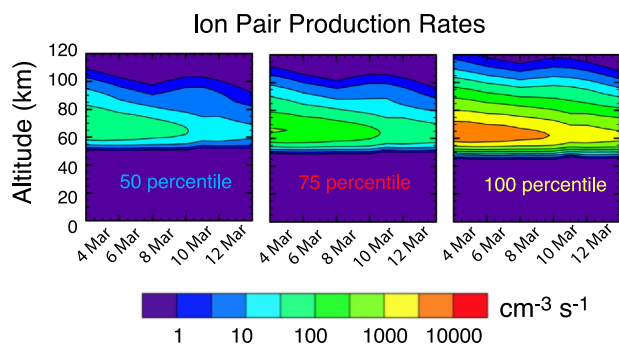


Figure 8. Ionization profiles using flux ratios representing the 50th (median), 75th, and 100th percentile ratios from the conjunction study (Figure 6) applied to Van Allen Probes electron flux at an L shell of five (Figure 7).

exceed 50% above 70 km for the median flux ratio case and 60%–70% extending down to 60 km for high flux ratio case. Changes in HO_x , NO_x , and O_3 using ionization rates from CMIP6 are similar to the median flux ratio simulations, particularly at higher altitudes.

In the weeks following the March 2013 event, the Northern Hemisphere polar vortex remains relatively stable, encouraging strong diabatic descent of enhanced NO_x into the stratosphere. Figure 11 depicts the boundary of the meandering polar vortex, objectively determined by identifying grid points within the stratosphere where scaled potential vorticity (sPV) on isentropic surfaces exceeds $1.4 \times 10^{-4} \text{ s}^{-1}$ (e.g., Brakebusch et al., 2013; Duderstadt et al., 2014; Dunkerton & Delisi, 1986). Scaled potential vorticity retains the conservation properties of Ertel's potential vorticity while being normalized with respect to the standard atmosphere. In the mesosphere, the vortex is assumed to extend to the same latitude as the top of the stratosphere, noting that the sPV method no longer adequately delineates the vortex edge given the temperature profile. During 2013, the winter polar vortex continues to persist throughout most of March, breaking up toward the end of the month.

Figure 12 shows the modeled enhancement of NO_x and reductions of O_3 averaged over the polar stratospheric vortex (sPV greater than $1.4 \times 10^{-4} \text{ s}^{-1}$) during the weeks following the March 2013 electron loss event. Enhancements of NO_x descending into the upper stratosphere (40–50 km) reach 20%–30% for the 50th percentile flux ratios and 80%–90% for the 100th percentile case and persist through April. Reductions of O_3 are only 1% for the 50th percentile case at 40–50 km but up to 40% for the 100th percentile case.

4. Discussion

During the storm recovery of early March 2013, we estimate that peak ionization rates from the precipitation of radiation belt electrons reach tens of ion pairs $\text{cm}^{-3} \text{ s}^{-1}$ in the altitude region of 60–80 km. For comparison, ion pair production from weak solar proton events is less than $1 \text{ cm}^{-3} \text{ s}^{-1}$. The most likely scenario, where MagEIS electron flux is scaled to median flux ratios derived from spacecraft conjunctions, results in 40% enhancements of NO_x averaged over the polar vortex from 60 to 70 km altitudes. CMIP6 APEEP simulations do not show similar levels of NO_x enhancement below 70 km during this time period, raising the question of whether APEEP underestimates electron precipitation in higher energy ranges. We remind readers that this study only considers NO_x enhancements from radiation belt electron precipitation during this unique March 2013 sustained electron decay event and does not address questions of enhancements

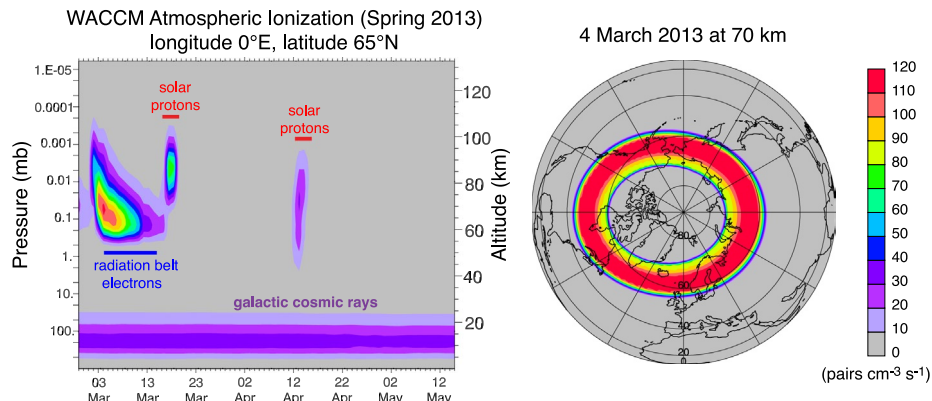


Figure 9. (a) Atmospheric ionization profiles used in the WACCM simulation involving solar protons, galactic cosmic rays, and estimated radiation belt electron precipitation using median (50th percentile) flux ratios. Radiation belt electrons are included from 26 February to 17 March 2013. (b) Atmospheric ionization at 70 km on 4 March 2013 for the 50th percentile flux ratio.

WACCM Simulations of March 2013 Electron Loss Event
 HO_x , NO_x , and $-\Delta\text{O}_3$ (65° N latitude, 0° E longitude)

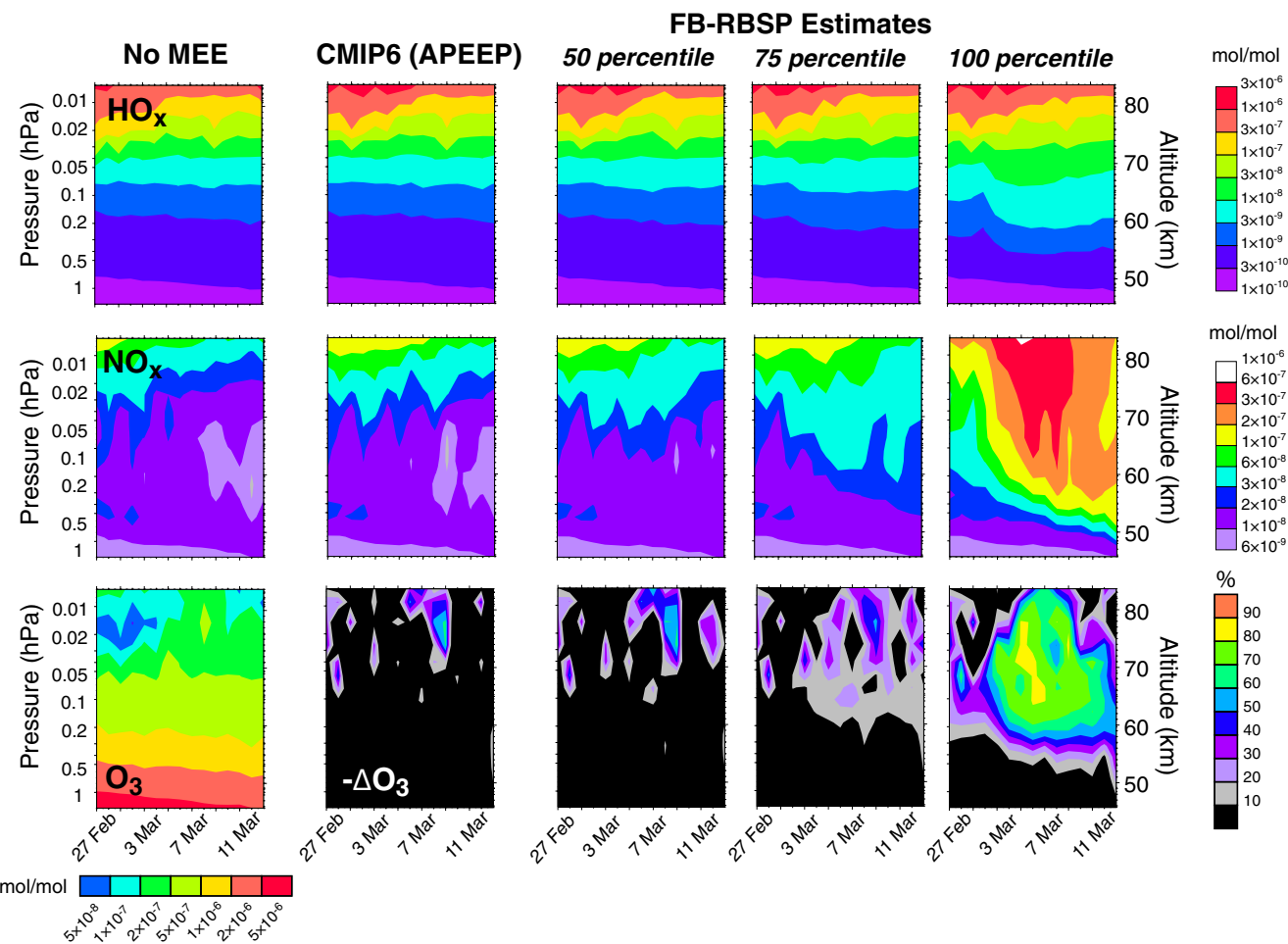


Figure 10. WACCM simulations for the March 2013 event showing localized enhancements of HO_x and NO_x and reductions of O_3 . Includes simulations without radiation belt electrons (No MEE), with CMIP6 ionization (CMIP6 APEEP), and with Van Allen Probes observations scaled to 50th, 75th, and 100th percentile flux ratios from the study of conjunctions between FIREBIRD II and the Van Allen Probes.

involving NO_x production and dynamics earlier in the winter. As this event coincides with a winter where the atmosphere is characterized by strong descent associated with a sudden stratospheric warming, we recognize that these circumstances make it challenging to determine if NO_x enhancements are the result of electron precipitation or dynamics.

During March 2013, NO observations from Odin/SMR show zonal average values poleward of 70°N ranging between 10 and 30 ppbv from 0.3 to 0.02 hPa (~ 55 –75 km) (see Figure 2b in Pérot et al., 2014). Since 2007, the Odin submillimeter radar, a limb emissions sounder, has been providing global sampling of NO with vertical resolution of ~ 7 km based on the thermal emission lines in the 551.7 GHz band. Our median flux ratio WACCM simulations compare well with Odin/SMR satellite observations, with enhancements of tens of ppbv persisting during and following the electron loss event (as evident in Figure 13).

Figure 13 shows comparisons of WACCM NO calculations along the track of the SOFIE-AIM observations (also presented in Bailey et al., 2014; Hendrickx et al., 2015). SOFIE solar occultation measurements are made for NO using the 5.32 μm absorption band, providing 15 sunrise measurements per day from 65°N to 85°N and 20–140 km (from 2007 until the present). Because our case studies involve electron precipitation beginning in March, they do not adequately address the confluence of processes leading to prominent

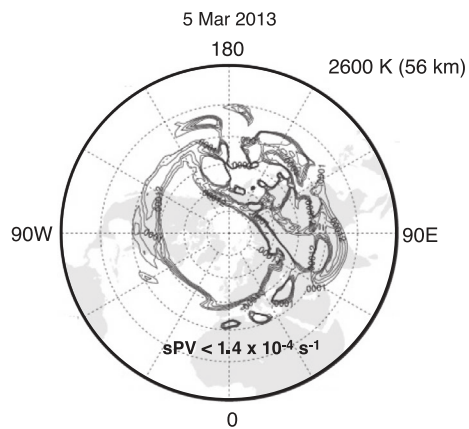


Figure 11. The location of the stratospheric polar vortex in the Northern Hemisphere near the start of the March 2013 electron decay event ($sPV > 1.4 \times 10^{-4} \text{ s}^{-1}$).

NO descent following the January 2013 sudden stratospheric warming (SSW). However, it is notable that WACCM simulations considering only solar protons and auroral electrons (WACCM no MEE) fail to reproduce the large and narrow enhancements in NO_x that descends below 50 km discussed in Bailey et al. (2014). Although our study focuses on NO_x production in the 1 to 0.01 hPa range during March 2013, questions remain regarding the competing roles of dynamics and the production of NO_x by MEE to explain discrepancies following SSWs (e.g., Hendrickx et al., 2018; Randall et al., 2015; Siskind et al., 2015). While Hendrickx et al. (2018) demonstrate good agreement in descent rates between WACCM and satellite observations (based on observations over the Southern Hemisphere), Siskind et al. (2015) show that adding data assimilation at higher altitudes results in NO predictions that better match satellite observations following the 2009 Northern Hemisphere SSW.

The SOFIE observations do not show similar enhancements between 60 and 70 km observed by ODIN and predicted by our WACCM 50th percentile flux ratio simulations during early March. However, SOFIE is also orbiting above 80°N during this time period, beyond latitudes corresponding to the outer radiation belt. Nonetheless, it is clear that the

extreme scenario (based on 100th percentile flux ratios) is unlikely, as the enhancements for that simulation are over 100 ppbv and should be large enough to be detected by ODIN and SOFIE. Therefore, precipitation of electrons into the atmosphere likely contributes to but does not dominate the loss observed within the radiation belts during the March event (the 95% reduction from peak levels according to TRBEC).

Figure 14 shows the atmospheric ionization used in CMIP6 simulations, representing the sum of ionization from solar protons, galactic cosmic rays, and the APEEP parameterization of electron precipitation. Except during the solar proton enhancements around 12 April and 20 May, there is very little ionization below 70 km, an altitude representing ionization from electrons with energies greater than ~300 keV. Van de Kamp et al. (2018) acknowledge the challenge of using POES MEPED instruments to estimate atmospheric ionization from higher energy electrons outside of high flux storm times. The method presented in this paper may enable a unique understanding of how significant these higher energy electrons are to atmospheric ionization and subsequent influences on NO_x and O_3 . However, comparing Figures 14 with 9 demonstrates that the MagEIS energy range used in this study (57 keV–1.7 MeV) also limits estimates of ionization at altitudes above 80 km, the region most often associated with longer-term downward transport of NO_x to the stratosphere and impacts to O_3 , a process often termed the “indirect effect” (e.g., Funke et al., 2014; Randall et al., 2007; Sinnhuber et al., 2018). The Van Allen Probes ECT team is currently developing a combined data product that includes data from the Helium Oxygen Proton Electron (HOPE) plasma spectrometer that will enable a better representation of electrons with energies below 50 keV (Boyd et al., 2019). We also recognize the challenges associated with the March 2013 case study following a winter of sudden stratospheric warming. It would be preferable to identify sustained electron loss events that occur during periods when it is easier to distinguish between NO_x enhancement from electron precipitation and atmospheric descent.

The calculated atmospheric impacts on NO_x and O_3 as a result of electron precipitation during the March 2013 electron loss event are relatively small, with lower estimates (median flux ratios) resulting in a decrease in O_3 in the upper stratosphere of ~1%. However, we should note that even a 1% decrease can disrupt the radiative and dynamic properties of the middle atmosphere (e.g., Rozanov et al., 2005; Seppälä et al., 2009; 2013; Lu et al., 2017). Furthermore, it is important to adequately represent direct production and background concentrations of NO_x at all altitudes, and enhanced ionization at altitudes lower than captured by CMIP APEEP is worthy of further study. The method also shows promise in capturing the longer duration of electron precipitation following HSSWS events, potentially underpredicted by the APEEP model (Nesse Tyssøy et al., 2019). In addition, while ratios of FIREBIRD II to Van Allen Probes observations during conjunctions show that, on average, 1%–2% of electrons observed within the 0°–8° pitch angles by the Van Allen Probes precipitate into the atmosphere, and there are times when this ratio approaches 90% at higher energies. It would be valuable to consider processes beyond daily average flux estimates, including

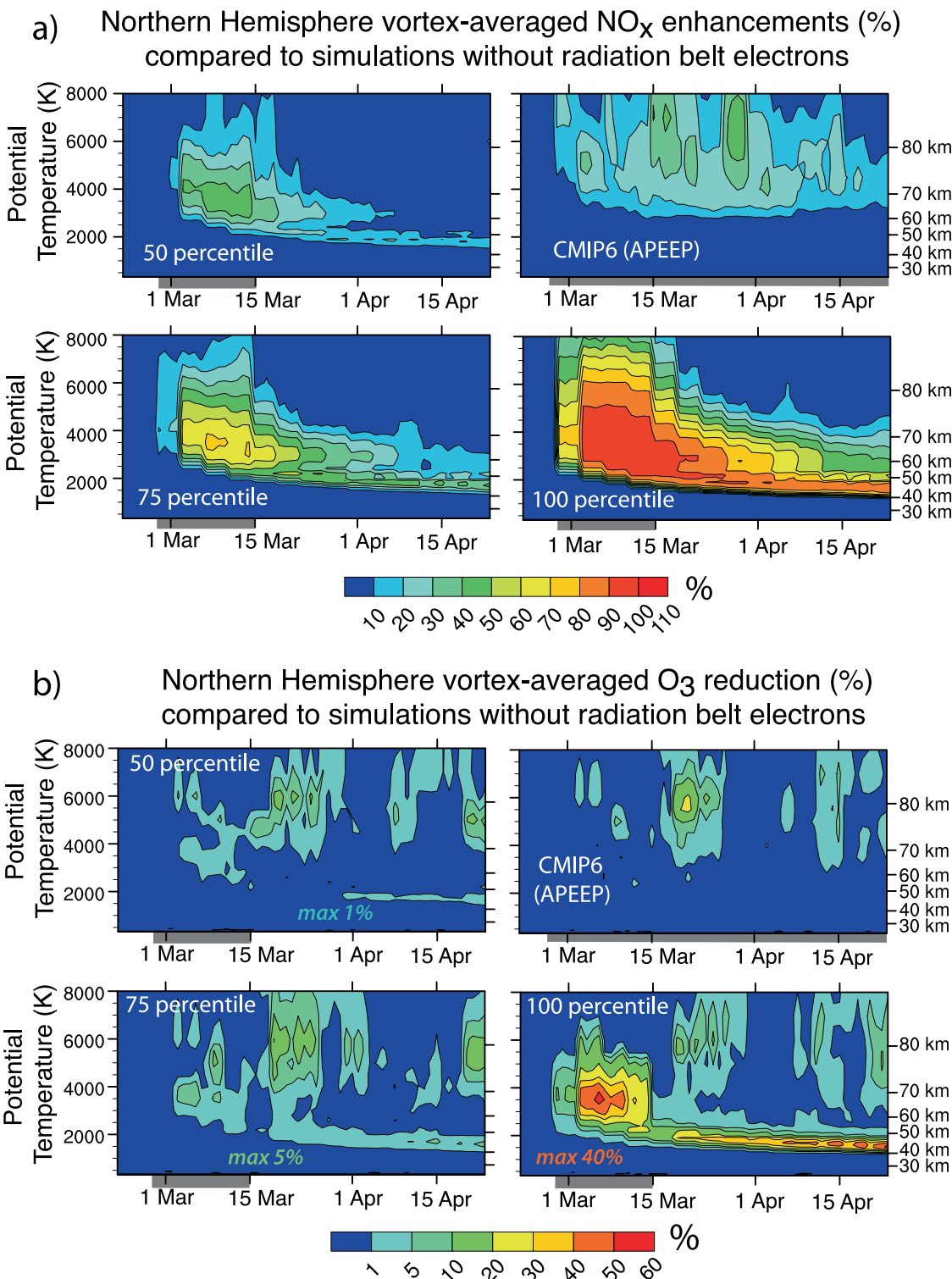


Figure 12. WACCM simulations for the March 2013 event showing longer term (a) enhancements of NO_x and (b) reductions of O_3 averaged over the Northern Hemisphere polar vortex from radiation belt electrons for each of the simulations. Gray bars represent times when MEE ionization is included in the simulations.

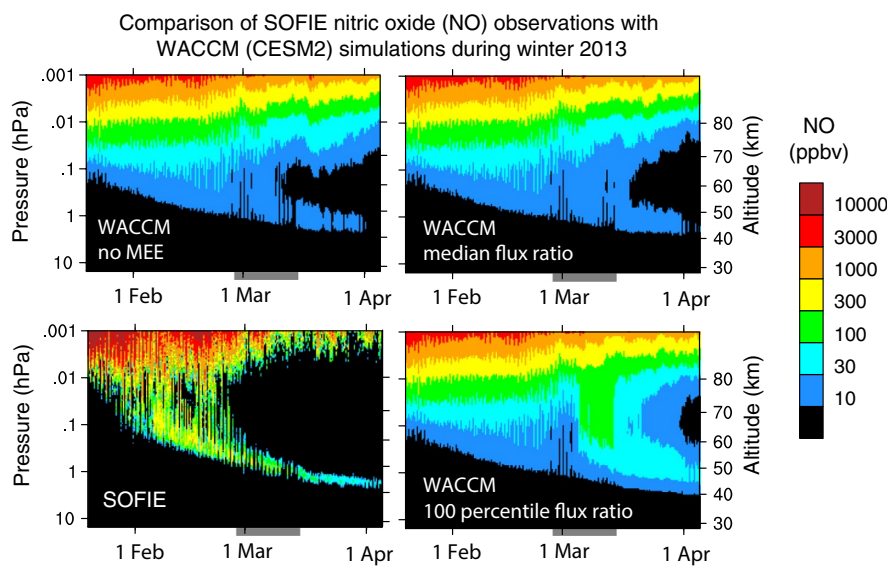


Figure 13. Northern Hemisphere comparison of the Solar Occultation for Ice Experiment (SOFIE) satellite observations of NO_x during winter 2013 with WACCM simulations of radiation belt electron precipitation (latitudes $>65^\circ\text{N}$). Black regions indicate NO values less than 10 ppbv. (SOFIE Level 2 Version 1.3 NO vmr data were downloaded from <http://sofie.gats-inc.com/sofie/>, retrieved August 2020.) Gray bars show times when MEE is included.

microburst clusters and precipitation bands (e.g., Blum et al., 2015; Greeley et al., 2019; Johnson et al., 2020) that have been shown to impact ionization calculated at lower altitudes (Seppälä et al., 2018). An additional option is to better estimate fluxes within the loss cone by extrapolating to smaller pitch angles based on pitch angle distributions (e.g., Gannon et al., 2007; Shi et al., 2016).

This study demonstrates the potential for using observations of electron distributions within the Van Allen Belts to estimate the fluence and spectral distributions of electron precipitation. Since August 2018, the FIREBIRD II team has been targeting high resolution downloads during conjunctions with the Van Allen Probes, providing a much larger and closer set of conjunctions for follow-up studies. Observations during conjunctions between POES satellites and FIREBIRD are also being downloaded to allow better comparisons of spectral shape. Future plans are to use the new methods outlined in this work to estimate electron precipitation over the entire Van Allen Probes mission. We also plan to conduct studies using a new “tagged NO_x ” chemical mechanism in WACCM (Marsh et al., 2018) to distinguish direct production of NO_x from radiation belt electrons, NO_x production by solar protons, and the descent of NO_x from auroral electrons. The pitch-angle resolved electron observations in LEO from the recently launched Electron Losses and Fields Investigation (ELFIN) CubeSat mission (Shprits et al., 2018) may enable additional understanding of these precipitation flux ratios.

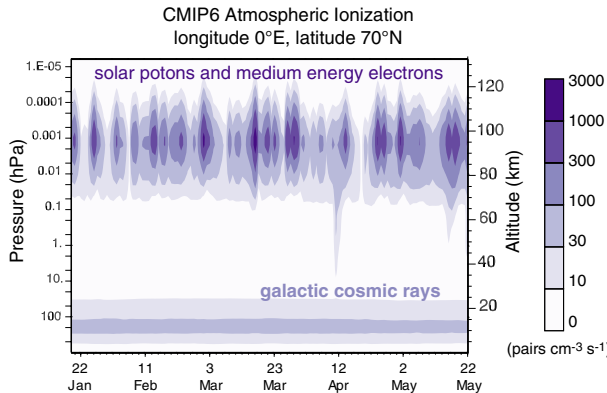


Figure 14. Ionization rates from The Coupled Model Intercomparison Project (CMIP6) that includes solar protons, galactic cosmic rays, and the APEEP parameterization of electron precipitation from January to May 2013. The location 70°N and 0°E represents a latitude of peak flux.

5. Conclusions

This study presents a new method of estimating electron precipitation from observations directly within the radiation belts. Electron flux measurements from the Van Allen Probes MageIS instrument are scaled to flux ratios determined from a study of spacecraft conjunctions with FIREBIRD-II CubeSats to create maps of electron precipitation. WACCM simulations using these maps of electron precipitation show enhancements of HO_x and NO_x and reductions of O_3 in the middle atmosphere, with the magnitude and altitude of these effects depending on the precipitating electron energy distribution.

A case study in early March 2013 represents a period of unusually long and sustained electron loss from the radiation belts during recovery from a moderate storm. While electron loss during the main phase of storms is generally attributed to loss through the magnetopause, we assume much of the electron decay during this unique sustained electron loss event is associated with precipitation into the atmosphere. WACCM simulations for this event, using electron precipitation based on median flux ratios derived from the conjunction study, show 40% enhancements of NO_x within 60–70 km and O_3 reductions of ~1% in the mid stratosphere during the weeks following the event. While changes to NO_x and O_3 are relatively small for this individual event, over longer timescales, there is the potential for many such events to alter the mean background composition. Odin/SMR satellite observations confirm enhancements of NO similar to values calculated at these altitudes by WACCM, highlighting the potential importance of low levels of electron flux at higher energies. This study suggests that the current APEEP parameterizations of MEE used in CMIP6, while remaining the best available option for long-term atmospheric modeling, may underestimate the duration of electron precipitation following HSSWS storms, as well as the contribution to atmospheric ionization from higher energy electrons producing NO_x at lower altitudes.

Our results motivate future plans to study the impact of electrons on atmospheric composition by developing electron precipitation maps throughout the extent of the Van Allen Probes mission (2012–2019), extending to lower electron energies based on the combined RBSP-ECT dataset (Boyd et al., 2019). We also plan to search for observations of sustained electron loss events within the radiation belts that occur outside of times with strong atmospheric descent. Electron precipitation maps will be compared with estimates derived from POES MEPED instruments that are currently being used to drive CMIP6 simulations through the APEEP parameterization (Matthes et al., 2017; van de Kamp, 2016) and will provide a unique estimate of atmospheric impacts of radiation belt electrons during the peak and descending portion of solar cycle 24. Efforts are also underway to conduct a more comprehensive analysis of spacecraft conjunctions among FIREBIRD II, Van Allen Probes, and POES to identify the radiation belt conditions that drive flux ratios and their energy dependence. This method of estimating atmospheric electron precipitation using observations from within the radiation belts will likely contribute new understandings to processes that couple Earth's magnetosphere and atmosphere.

Data Availability Statement

WACCM6 code is available as part of the CESM2 release via github. Instructions are at this site (http://www.cesm.ucar.edu/models/cesm2/release_download.html). Computing and data storage resources, including the Cheyenne supercomputer (<http://doi.org/10.5065/D6RX99HX>), are provided by the Computational and Information Systems Laboratory (CISL) at NCAR. Van Allen Probes data is available at <http://rbspgway.jhuapl.edu/>. FIREBIRD II data is available at http://solar.physics.montana.edu/FIREBIRD_II/ and was made possible by NSF (Nos. 0838034 and 1339414). Additional data files specific to this study are available on the Harvard Dataverse at <https://doi.org/10.7910/DVN/QCDYHI>.

Acknowledgments

This research was supported by NSF (Nos. 1650738, 1650918, and 1035642) and NASA (No. 135260). The CESM project was supported primarily by the National Science Foundation.

References

Andersson, M. E., Verronen, P. T., Marsh, D. R., Päivärinta, S.-M., & Plane, J. M. C. (2016). WACCM-D—Improved modeling of nitric acid and active chlorine during energetic particle precipitation. *Journal of Geophysical Research: Atmospheres*, 121, 10328–10341. <https://doi.org/10.1002/2015jd024173>

Andersson, M. E., Verronen, P. T., Marsh, D. R., Seppälä, A., Päivärinta, S.-M., Rodger, C. J., et al. (2018). Polar ozone response to energetic particle precipitation over decadal time scales: The role of medium-energy electrons. *Journal of Geophysical Research - D: Atmospheres*, 123, 607–622. <https://doi.org/10.1002/2017jd027605>

Andersson, M. E., Verronen, P. T., Rodger, C. J., Clilverd, M. A., & Seppälä, A. (2014). Missing driver in the Sun–Earth connection from energetic electron precipitation impacts mesospheric ozone. *Nature Communications*, 5, 5197. <https://doi.org/10.1038/ncomms6197>

Andersson, M. E., Verronen, P. T., Rodger, C. J., Clilverd, M. A., & Wang, S. (2014). Longitudinal hotspots in the mesospheric OH variations due to energetic electron precipitation. *Atmospheric Chemistry and Physics*, 14, 1095–1105. <https://doi.org/10.5194/acp-14-1095-2014>

Arsenovic, P., Rozanov, E., Stenke, A., Funke, B., Wissing, J. M., Mursula, K., et al. (2016). The influence of middle range energy electrons on atmospheric chemistry and regional climate. *Journal of Atmospheric and Solar-Terrestrial Physics*, 149, 180–190. <https://doi.org/10.1016/j.jastp.2016.04.008>

Artamonov, A. A., Mishev, A. L., & Usoskin, I. G. (2016). Atmospheric ionization induced by precipitating electrons: Comparison of CRAC:EPII model with a parametrization model. *Journal of Atmospheric and Solar-Terrestrial Physics*. <https://doi.org/10.1016/j.jastp.2016.04.020>

Artamonov, A., Mironova, I., Kovaltsov, G., Mishev, A., Plotnikov, E., & Konstantinova, N. (2017). Calculation of atmospheric ionization induced by electrons with non-vertical precipitation: Updated model CRAC-EPII. *Advances in Space Research*, 59(9), 2295–2300. <https://doi.org/10.1016/j.asr.2017.02.019>

Bailey, S. M., Thurairajah, B., Randall, C. E., Holt, L., Siskind, D. E., Harvey, V. L., et al. (2014). A multi tracer analysis of thermosphere to stratosphere descent triggered by the 2013 Stratospheric Sudden Warming. *Geophysical Research Letters*, 41, 5216–5222. <https://doi.org/10.1002/2014gl059860>

Baker, D. N., Jaynes, A. N., Li, X., Henderson, M. G., Kanekal, S. G., Reeves, G. D., et al. (2014). Gradual diffusion and punctuated phase space density enhancements of highly relativistic electrons: Van Allen Probes observations. *Geophysical Research Letters*, 41, 1351–1358. <https://doi.org/10.1002/2013gl058942>

Baumgaertner, A. J. G., Seppälä, A., Jöckel, P., & Clilverd, M. A. (2011). Geomagnetic activity related NO_x enhancements and polar surface air temperature variability in a chemistry climate model: modulation of the NAM index. *Atmospheric Chemistry and Physics*, 11, 4521–4531. <https://doi.org/10.5194/acp-11-4521-2011>

Blake, J. B., Carranza, P. A., Claudepierre, S. G., Clemons, J. H., Crain, W. R., Dotan, Y., et al. (2013). The magnetic electron ion spectrometer (MagEIS) instruments aboard the radiation belt storm probes (RBSP), spacecraft. *Space Science Reviews*. <https://doi.org/10.1007/s11214-013-9991-8>

Blum, L., Li, X., & Denton, M. (2015). Rapid MeV electron precipitation as observed by SAMPEX/HILT during high-speed stream-driven storms. *Journal of Geophysical Research: Space Physics*, 120, 3783–3794. <https://doi.org/10.1002/2014ja020633>

Boyd, A. J., Reeves, G. D., Spence, H. E., Funsten, H. O., Larsen, B. A., Skoug, R. M., et al. (2019). RBSP-ECT Combined Spin-Averaged Electron Flux Data Product. *Journal of Geophysical Research: Space Physics*, 124, 9124–9136. <https://doi.org/10.1029/2019ja026733>

Brakebusch, M., Randall, C. E., Kinnison, D. E., Tilmes, S., Santee, M. L., & Manney, G. L. (2013). Evaluation of Whole Atmosphere Community Climate Model simulations of ozone during Arctic winter 2004–2005. *Journal of Geophysical Research - D: Atmospheres*, 118, 2673–2688. <https://doi.org/10.1002/jgrd.50226>

Callis, L. B., Baker, D. N., Blake, J. B., Lambeth, J. D., Boughner, R. E., Natarajan, M., et al. (1991). Precipitating relativistic electrons: Their long-term effect on stratospheric odd nitrogen levels. *Journal of Geophysical Research*, 96(D2), 2939–2976. <https://doi.org/10.1029/90jd02184>

Charlton-Perez, A. J., Baldwin, M. P., Birner, T., Black, R. X., Butler, A. H., Calvo, N., et al. (2013). On the lack of stratospheric dynamical variability in low-top versions of the CMIP5 models. *Journal of Geophysical Research - D: Atmospheres*, 118(6), 2494–2505. <https://doi.org/10.1002/jgrd.50125>

Clilverd, M. A., Rodger, C. J., & Ulich, T. (2006). The importance of atmospheric precipitation in storm-time relativistic electron flux drop outs. *Geophysical Research Letters*, 33. <https://doi.org/10.1029/2005gl024661>

Clilverd, M. A., Rodger, C. J., van de Kamp, M., & Verrenen, P. T. (2020). Electron precipitation from the outer radiation belt during the St. Patrick's day storm 2015: Observations, modeling, and validation. *Journal of Geophysical Research: Space Physics*, 125, e2019JA027725. <https://doi.org/10.1029/2019ja027725>

Clilverd, M. A., Seppälä, A., Rodger, C. J., Mlynczak, M. G., & Kozyra, J. U. (2009). Additional stratospheric NO_x production by relativistic electron precipitation during the 2004 spring NO_x descent event. *Journal of Geophysical Research: Space Physics*, 114. <https://doi.org/10.1029/2008ja013472>

Codrescu, M. V., Fuller-Rowell, T. J., Roble, R. G., & Evans, D. S. (1997). Medium energy particle precipitation influences on the mesosphere and lower thermosphere. *Journal of Geophysical Research*, 102(A9), 19977–19987. <https://doi.org/10.1029/97ja01728>

Crew, A. B., Spence, H. E., Blake, J. B., Klumpar, D. M., Larsen, B. A., O'Brien, T. P., et al. (2016). First multipoint in situ observations of electron microbursts: Initial results from the NSF FIREBIRD II mission. *Journal of Geophysical Research: Space Physics*, 121(6), 5272–5283. <https://doi.org/10.1002/2016ja022485>

Duderstadt, K. A., Dibb, J. E., Jackman, C. H., Randall, C. E., Solomon, S. C., Mills, M. J., et al. (2014). Nitrate deposition to surface snow at Summit, Greenland, following the 9 November 2000 solar proton event. *Journal of Geophysical Research - D: Atmospheres*, 119, 6938–6957. <https://doi.org/10.1002/2013jd021389>

Duderstadt, K. A., Dibb, J. E., Schwadron, N. A., Spence, H. E., Solomon, S. C., Yudin, V. A., et al. (2016). Nitrate ion spikes in ice cores not suitable as proxies for solar proton events. *Journal of Geophysical Research: Atmospheres*, 121, 2994–3016. <https://doi.org/10.1002/2015JD023805>

Dunkerton, T. J., & Delisi, D. P. (1986). Evolution of potential vorticity in the winter stratosphere of January–February 1979. *Journal of Geophysical Research*, 91(D1), 1199–1208. <https://doi.org/10.1029/jd091id01p01199>

Fang, X., Randall, C. E., Lummertzheim, D., Wang, W., Lu, G., Solomon, S. C., & Fahrm, R. A. (2010). Parameterization of monoenergetic electron impact ionization. *Geophysical Research Letters*, 37(22), L22106. <https://doi.org/10.1029/2010gl045406>

Forsyth, C., Rae, I. J., Murphy, K. R., Freeman, M. P., Huang, C.-L., Spence, H. E., et al. (2016). What effect do substorms have on the content of the radiation belts? *Journal of Geophysical Research: Space Physics*, 121, 6292–6306. <https://doi.org/10.1002/2016ja022620>

Funke, B., Baumgaertner, A., Calisto, M., Egorova, T., Jackman, C. H., Kieser, J., et al. (2011). Composition changes after the “Halloween” solar proton event: The High Energy Particle Precipitation in the Atmosphere (HEPPA) model versus MIPAS data intercomparison study. *Atmospheric Chemistry and Physics*, 11(17), 9089–9139. <https://doi.org/10.5194/acp-11-9089-2011>

Funke, B., López-Puertas, M., Holt, L., Randall, C. E., Stiller, G. P., & von Clarmann, T. (2014). Hemispheric distributions and interannual variability of NO_y produced by energetic particle precipitation in 2002–2012. *Journal of Geophysical Research: Atmospheres*, 119, 13565–13582. <https://doi.org/10.1002/2014jd022423>

Gaines, E. E., Chenette, D. L., Imhof, W. L., Jackman, C. H., & Winningham, J. D. (1995). Relativistic electron fluxes in May 1992 and their effect on the middle atmosphere. *Journal of Geophysical Research*, 100, 1027–1033. <https://doi.org/10.1029/94jd02615>

Gannon, J. L., Li, X., & Heynderickx, D. (2007). Pitch angle distribution analysis of radiation belt electrons based on combined release and radiation effects satellite medium electrons A data. *Journal of Geophysical Research: Space Physics*, 112. <https://doi.org/10.1029/2005ja011565>

Garcia, R. R., Marsh, D. R., Kinnison, D. E., Boville, B. A., & Sassi, F. (2007). Simulation of secular trends in the middle atmosphere, 1950–2003. *Journal of Geophysical Research: Atmospheres*, 112(D9), D09301. <https://doi.org/10.1029/2006jd007485>

Gelaro, R., McCarty, W., Suárez, M. J., Todling, R., Molod, A., Takacs, L., et al. (2017). The modern-era retrospective analysis for research and applications, version 2 (MERRA-2). *Journal of Climate*, 30, 5419–5454. <https://doi.org/10.1175/jcli-d-16-0758.1>

Gerontidou, M., Mavromichalaki, H., & Daglis, T. (2018). High-speed solar wind streams and geomagnetic storms during solar cycle 24. *Solar Physics*, 293, 131. <https://doi.org/10.1007/s11207-018-1348-8>

Gettelman, A., Mills, M. J., Kinnison, D. E., Garcia, R. R., Smith, A. K., Marsh, D. R., et al. (2019). The whole atmosphere community climate model version 6 (WACCM6). *Journal of Geophysical Research: Atmospheres*, 124, 12380–12403. <https://doi.org/10.1029/2019jd030943>

Gordley, L. L., Hervig, M. E., Fish, C., Russell, J. M., Bailey, S., Cook, J., et al. (2009). The solar occultation for ice experiment. *Journal of Atmospheric and Solar-Terrestrial Physics*, 71, 300–315. <https://doi.org/10.1016/j.jastp.2008.07.012>

Greeley, A. D., Kanekal, S. G., Baker, D. N., Klecker, B., & Schiller, Q. (2019). Quantifying the contribution of microbursts to global electron loss in the radiation belts. *Journal of Geophysical Research: Space Physics*, 124, 1111–1124. <https://doi.org/10.1029/2018ja026368>

Hartley, D. P., & Denton, M. H. (2014). Solving the radiation belt riddle. *Astronomy and Geophysics*, 55, 6.17–6.20. <https://doi.org/10.1093/astropgeo/atu247>

Hendrickx, K., Megner, L., Gumbel, J., Siskind, D. E., Orsolini, Y. J., Tysseøy, H. N., & Hervig, M. (2015). Observation of 27 day solar cycles in the production and mesospheric descent of EPP-produced NO. *Journal of Geophysical Research: Space Physics*, 120, 8978–8988. <https://doi.org/10.1002/2015ja021441>

Hendrickx, K., Megner, L., Marsh, D. R., & Smith-Johnsen, C. (2018). Production and transport mechanisms of NO in the polar upper mesosphere and lower thermosphere in observations and models. *Atmospheric Chemistry and Physics*, 18, 9075–9089. <https://doi.org/10.5194/acp-18-9075-2018>

Jackman, C. H., Frederick, J. E., & Stolarski, R. S. (1980). Production of odd nitrogen in the stratosphere and mesosphere: An intercomparison of source strengths. *Journal of Geophysical Research*, 85(C12), 7495–7505. <https://doi.org/10.1029/jc085ic12p07495>

Jackman, C. H., Marsh, D. R., Vitt, F. M., Garcia, R. R., Fleming, E. L., Labow, G. J., et al. (2008). Short- and medium-term atmospheric constituent effects of very large solar proton events. *Atmospheric Chemistry and Physics*, 8(3), 765–785. <https://doi.org/10.5194/acp-8-765-2008>

Jackman, C. H., Marsh, D. R., Vitt, F. M., Garcia, R. R., Randall, C. E., Fleming, E. L., & Frith, S. M. (2009). Long-term middle atmospheric influence of very large solar proton events. *Journal of Geophysical Research: Atmospheres*, 114. <https://doi.org/10.1029/2008jd011415>

Johnson, A. T., Shumko, M., Griffith, B., Klumpar, D. M., Sample, J., Springer, L., et al. (2020). The FIREBIRD-II CubeSat mission: Focused investigations of relativistic electron burst intensity, range, and dynamics. *Review of Scientific Instruments*, 91, 034503. <https://doi.org/10.1063/1.5137905>

Kanekal, S. G., Baker, D. N., & Blake, J. B. (2001). Multisatellite measurements of relativistic electrons: Global coherence. *Journal of Geophysical Research*, 106, 29721–29732. <https://doi.org/10.1029/2001ja000070>

Lam, M. M., Horne, R. B., Meredith, N. P., Glauert, S. A., Moffat-Griffin, T., & Green, J. C. (2010). Origin of energetic electron precipitation >30 keV into the atmosphere. *Journal of Geophysical Research: Space Physics*, 115, A00F08. <https://doi.org/10.1029/2009ja014619>

Li, Z., Hudson, M., Jaynes, A., Boyd, A., Malaspina, D., Thaller, S., et al. (2014). Modeling gradual diffusion changes in radiation belt electron phase space density for the March 2013 Van Allen Probes case study. *Journal of Geophysical Research: Space Physics*, 119, 8396–8403. <https://doi.org/10.1002/2014ja020359>

Lorentzen, K. R.,Looper, M. D., & Blake, J. B. (2001). Relativistic electron microbursts during the GEM storms. *Geophysical Research Letters*, 28, 2573–2576. <https://doi.org/10.1029/2001gl012926>

Lu, H., Scaife, A. A., Marshall, G. J., Turner, J., & Gray, L. J. (2017). Downward wave reflection as a mechanism for the stratosphere-troposphere response to the 11-Yr solar cycle. *Journal of Climate*, 30, 2395–2414. <https://doi.org/10.1175/jcli-d-16-0400.1>

Marsh, D., Kinnison, D., & Lamarque, J.-F. (2018). Quantifying the energetic particle precipitation influences on the budgets of stratospheric NO_y and ozone using a new “tagging” scheme in the Whole Atmosphere Community Climate Model, 20th EGU General Assembly, EGU2018. *Paper presented at Proceedings from the conference held 4–13 April, 2018*, p. 3534.

Marsh, D. R., Garcia, R. R., Kinnison, D. E., Boville, B. A., Sassi, F., Solomon, S. C., & Matthes, K. (2007). Modeling the whole atmosphere response to solar cycle changes in radiative and geomagnetic forcing. *Journal of Geophysical Research: Atmospheres*, 112(D23), D23306. <https://doi.org/10.1029/2006jd008306>

Marsh, D. R., Mills, M. J., Kinnison, D. E., Lamarque, J.-F., Calvo, N., & Polvani, L. M. (2013). Climate change from 1850 to 2005 simulated in CESM1(WACCM). *Journal of Climate*, 26(19), 7372–7391. <https://doi.org/10.1175/jcli-d-12-00558.1>

Matthes, K., Funke, B., Andersson, M. E., Barnard, L., Beer, J., Charbonneau, P., et al. (2017). Solar forcing for CMIP6 (v3.2). *Geoscientific Model Development*, 10, 2247–2302. <https://doi.org/10.5194/gmd-10-2247-2017>

Millan, R. M., Lin, R. P., Smith, D. M., & McCarthy, M. P. (2007). Observation of relativistic electron precipitation during a rapid decrease of trapped relativistic electron flux. *Geophysical Research Letters*, 34. <https://doi.org/10.1029/2006gl028653>

Millan, R. M., McCarthy, M. P., Sample, J. G., Smith, D. M., Thompson, L. D., McGaw, D. G., et al. (2013). The balloon array for RBSP relativistic electron losses (BARREL). *Space Science Reviews*, 179, 503–530. <https://doi.org/10.1007/s11214-013-0781-5>

Millan, R. M., & Thorne, R. M. (2007). Review of radiation belt relativistic electron losses. *Journal of Atmospheric and Solar-Terrestrial Physics*, 69, 362–377. <https://doi.org/10.1016/j.jastp.2006.06.019>

Morley, S. K., Friedel, R. H. W., Spanswick, E. L., Reeves, G. D., Steinberg, J. T., Koller, J., et al. (2010). Dropouts of the outer electron radiation belt in response to solar wind stream interfaces: Global positioning system observations. *Proceedings of the Royal Society A: Mathematical, Physical and Engineering Sciences*, 466, 3329–3350. <https://doi.org/10.1098/rspa.2010.0078>

Murphy, K. R., Watt, C. E. J., Mann, I. R., Jonathan Rae, I., Sibeck, D. G., Boyd, A. J., et al. (2018). The global statistical response of the outer radiation belt during geomagnetic storms. *Geophysical Research Letters*, 45, 3783–3792. <https://doi.org/10.1002/2017gl076674>

Nesse Tysseøy, H., Haderlein, A., Sandanger, M. I., & Stadsnes, J. (2019). Intercomparison of the POES/MEPED loss cone electron fluxes with the CMIP6 Parametrization. *Journal of Geophysical Research: Space Physics*, 124, 628–642. <https://doi.org/10.1029/2018JA025745>

Nesse Tysseøy, H., Sandanger, M. I., Ødegaard, L.-K. G., Stadsnes, J., Aasnes, A., & Zawedde, A. E. (2016). Energetic electron precipitation into the middle atmosphere—Constructing the loss cone fluxes from MEPED POES. *Journal of Geophysical Research: Space Physics*, 121(6), 5693–5707. <https://doi.org/10.1002/2016JA022752>

Newnham, D. A., Clilverd, M. A., Rodger, C. J., Hendrickx, K., Megner, L., Kavanagh, A. J., et al. (2018). Observations and modeling of increased nitric oxide in the antarctic polar middle atmosphere associated with geomagnetic storm-driven energetic electron precipitation. *Journal of Geophysical Research: Space Physics*, 123, 6009–6025. <https://doi.org/10.1029/2018ja025507>

Newnham, D. A., Rodger, C. J., Marsh, D. R., Hervig, M. E., & Clilverd, M. A. (2020). Spatial distributions of nitric oxide in the antarctic wintertime middle atmosphere during geomagnetic storms. *Journal of Geophysical Research: Space Physics*, 125, e2020JA027846. <https://doi.org/10.1029/2020ja027846>

O'Brien, T. P.,Looper, M. D., & Blake, J. B. (2004). Quantification of relativistic electron microburst losses during the GEM storms. *Geophysical Research Letters*, 31. <https://doi.org/10.1029/2003GL018621>

Peck, E. D. (2014). *Impacts of energetic electron precipitation on the middle atmosphere*. University of Colorado at Boulder. Retrieved from <http://gradworks.umi.com/36/72/3672476.html>

Peck, E. D., Randall, C. E., Green, J. C., Rodriguez, J., & Rodger, C. J. (2015). POES MEPED differential flux retrievals and electron channel contamination correction. *Journal of Geophysical Research: Space Physics*, 120(6), 2014JA020817. <https://doi.org/10.1002/2014ja020817>

Pérot, K., Urban, J., & Murtagh, D. P. (2014). Unusually strong nitric oxide descent in the Arctic middle atmosphere in early 2013 as observed by Odin/SMR. *Atmospheric Chemistry and Physics*, 14, 8009–8015. <https://doi.org/10.5194/acp-14-8009-2014>

Pettitt, J. M., Randall, C. E., Peck, E. D., Marsh, D. R., Kamp, M., Fang, X., et al. (2019). Atmospheric effects of >30-keV energetic electron precipitation in the Southern Hemisphere winter during 2003. *Journal of Geophysical Research: Space Physics*, 124, 8138–8153. <https://doi.org/10.1029/2019ja026868>

Randall, C. E., Harvey, V. L., Holt, L. A., Marsh, D. R., Kinnison, D., Funke, B., & Bernath, P. F. (2015). Simulation of energetic particle precipitation effects during the 2003–2004 Arctic winter. *Journal of Geophysical Research: Space Physics*, 120(6), 5035–5048. <https://doi.org/10.1002/2015ja021196>

Randall, C. E., Harvey, V. L., Manney, G. L., Orsolini, Y., Codrescu, M., Sioris, C., et al. (2005). Stratospheric effects of energetic particle precipitation in 2003–2004. *Geophysical Research Letters*, 32(5), L05802. <https://doi.org/10.1029/2004gl022003>

Randall, C. E., Harvey, V. L., Singleton, C. S., Bailey, S. M., Bernath, P. F., Codrescu, M., et al. (2007). Energetic particle precipitation effects on the Southern Hemisphere stratosphere in 1992–2005. *Journal of Geophysical Research: Atmospheres*, 112. <https://doi.org/10.1029/2006jd007696>

Reeves, G. D., Friedel, R. H. W., Larsen, B. A., Skoug, R. M., Funsten, H. O., Claudepierre, S. G., et al. (2016). Energy-dependent dynamics of keV to MeV electrons in the inner zone, outer zone, and slot regions. *Journal of Geophysical Research: Space Physics*, 121, 397–412. <https://doi.org/10.1002/2015ja021569>

Reeves, G. D., McAdams, K. L., Friedel, R. H. W., & O'Brien, T. P. (2003). Acceleration and loss of relativistic electrons during geomagnetic storms. *Geophysical Research Letters*, 30. <https://doi.org/10.1029/2002gl016513>

Richardson, I. G., Cliver, E. W., & Cane, H. V. (2000). Sources of geomagnetic activity over the solar cycle: Relative importance of coronal mass ejections, high-speed streams, and slow solar wind. *Journal of Geophysical Research*, 105, 18203–18213. <https://doi.org/10.1029/1999ja000400>

Ripoll, J.-F., Reeves, G. D., Cunningham, G. S., Loridan, V., Denton, M., Santolík, O., et al. (2016). Reproducing the observed energy-dependent structure of Earth's electron radiation belts during storm recovery with an event-specific diffusion model. *Geophysical Research Letters*, 43, 5616–5625. <https://doi.org/10.1002/2016gl068869>

Roble, R. G., & Ridley, E. C. (1987). An auroral model for the NCAR thermospheric general circulation model (TGCM). *Annales Geophysicae*, 5, 369–382

Rodger, C. J., Clilverd, M. A., Green, J. C., & Lam, M. M. (2010). Use of POES SEM-2 observations to examine radiation belt dynamics and energetic electron precipitation into the atmosphere. *Journal of Geophysical Research: Space Physics*, 115(A4), A04202. <https://doi.org/10.1029/2008ja014023>

Rodger, C. J., Clilverd, M. A., Thomson, N. R., Gamble, R. J., Seppälä, A., Turunen, E., et al. (2007). Radiation belt electron precipitation into the atmosphere: Recovery from a geomagnetic storm. *Journal of Geophysical Research: Space Physics*, 112. <https://doi.org/10.1029/2007ja012383>

Rodger, C. J., Kavanagh, A. J., Clilverd, M. A., & Marple, S. R. (2013). Comparison between POES energetic electron precipitation observations and riometer absorptions: Implications for determining true precipitation fluxes. *Journal of Geophysical Research: Space Physics*, 118, 7810–7821. <https://doi.org/10.1002/2013ja019439>

Rozanov, E., Calisto, M., Egorova, T., Peter, T., & Schmutz, W. (2012). Influence of the precipitating energetic particles on atmospheric chemistry and climate. *Surveys in Geophysics*, 33, 483–501. <https://doi.org/10.1007/s10712-012-9192-0>

Rozanov, E. V., Callis, L. B., Schlesinger, M., Yang, F., Andronova, N., & Zubov, V. A. (2005). Atmospheric response to NO_y source due to energetic electron precipitation. *Geophysical Research Letters*, 32, L14811. <https://doi.org/10.1029/2005gl023041>

Selesnick, R. S. (2006). Source and loss rates of radiation belt relativistic electrons during magnetic storms. *Journal of Geophysical Research: Space Physics*, 111(A4), A04210. <https://doi.org/10.1029/2005ja011473>

Selesnick, R. S., Blake, J. B., & Mewaldt, R. A. (2003). Atmospheric losses of radiation belt electrons. *Journal of Geophysical Research: Space Physics*, 108. <https://doi.org/10.1029/2003ja010160>

Seppälä, A., Douma, E., Rodger, C. J., Verronen, P. T., Clilverd, M. A., & Bortnik, J. (2018). Relativistic electron microburst events: Modeling the atmospheric impact. *Geophysical Research Letters*, 45, 1141–1147. <https://doi.org/10.1002/2017gl075949>

Seppälä, A., Lu, H., Clilverd, M. A., & Rodger, C. J. (2013). Geomagnetic activity signatures in wintertime stratosphere wind, temperature, and wave response. *Journal of Geophysical Research - D: Atmospheres*, 118, 2169–2183. <https://doi.org/10.1002/jgrd.50236>

Seppälä, A., Randall, C. E., Clilverd, M. A., Rozanov, E. V., & Rodger, C. J. (2009). Geomagnetic activity and polar surface air temperature variability. *Journal of Geophysical Research*, 114, 10312. <https://doi.org/10.1029/2008ja014029>

Shi, R., Summers, D., Ni, B., Fennell, J. F., Blake, J. B., Spence, H. E., & Reeves, G. D. (2016). Survey of radiation belt energetic electron pitch angle distributions based on the Van Allen Probes MagEIS measurements. *Journal of Geophysical Research: Space Physics*, 121, 1078–1090. <https://doi.org/10.1002/2015ja021724>

Shprits, Y. Y., Angelopoulos, V., Russell, C. T., Strangeway, R. J., Runov, A., Turner, D., et al. (2018). Scientific objectives of electron losses and fields investigation onboard Lomonosov satellite. *Space Science Reviews*, 214(1), 25. <https://doi.org/10.1007/s11214-017-0455-4>

Shumko, M., Sample, J., Johnson, A., Blake, B., Crew, A., Spence, H., et al. (2018). Microburst scale size derived from multiple bounces of a microburst simultaneously observed with the FIREBIRD-II CubeSats. *Geophysical Research Letters*, 45, 8811–8818. <https://doi.org/10.1029/2018gl078925>

Sinnhuber, B.-M., von der Gathen, P., Sinnhuber, M., Rex, M., König-Langlo, G., & Oltmans, S. J. (2006). Large decadal scale changes of polar ozone suggest solar influence. *Atmospheric Chemistry and Physics*, 6(7), 1835–1841. <https://doi.org/10.5194/acp-6-1835-2006>

Sinnhuber, M., Berger, U., Funke, B., Nieder, H., Reddmann, T., Stiller, G., et al. (2018). NO_y production, ozone loss and changes in net radiative heating due to energetic particle precipitation in 2002–2010. *Atmospheric Chemistry and Physics*, 18, 1115–1147. <https://doi.org/10.5194/acp-18-1115-2018>

Sinnhuber, M., Nieder, H., & Wieters, N. (2012). Energetic particle precipitation and the chemistry of the mesosphere/lower thermosphere. *Surveys in Geophysics*, 33(6), 1281–1334. <https://doi.org/10.1007/s10712-012-9201-3>

Siskind, D. E., Sassi, F., Randall, C. E., Harvey, V. L., Hervig, M. E., & Bailey, S. M. (2015). Is a high-altitude meteorological analysis necessary to simulate thermosphere-stratosphere coupling? *Geophysical Research Letters*, 42, 8225–8230. <https://doi.org/10.1002/2015gl065838>

Smith-Johnsen, C., Marsh, D. R., Orsolini, Y., Tyssøy, H. N., Hendrickx, K., Sandanger, M. I., et al. (2018). Nitric oxide response to the April 2010 electron precipitation event: Using WACCM and WACCM-D with and without medium-energy electrons. *Journal of Geophysical Research: Space Physics*, 123, 5232–5245. <https://doi.org/10.1029/2018JA025418>

Smith-Johnsen, C., Tyssøy, H. N., Hendrickx, K., Orsolini, Y., Kumar, G. K., Ødegaard, L.-K. G., et al. (2017). Direct and indirect electron precipitation effect on nitric oxide in the polar middle atmosphere, using a full-range energy spectrum. *Journal of Geophysical Research: Space Physics*, 122, 8679–8693. <https://doi.org/10.1002/2017JA024364>

Spence, H. E., Blake, J. B., Crew, A. B., Driscoll, S., Klumpar, D. M., Larsen, B. A., et al. (2012). Focusing on size and energy dependence of electron microbursts from the Van Allen radiation belts. *Space Weather*, 10. <https://doi.org/10.1029/2012sw000869>

Spence, H. E., Reeves, G. D., Baker, D. N., Blake, J. B., Bolton, M., Bourdarie, S., et al. (2013). Science goals and overview of the radiation belt storm probes (RBSP) energetic particle, composition, and thermal plasma (ECT) suite on NASA's Van Allen Probes mission. *Space Science Reviews*, 179(1–4), 311–336. https://doi.org/10.1007/978-1-4899-7433-4_10

Stratton, J. M., Harvey, R. J., & Heyler, G. A. (2013). Mission overview for the radiation belt storm probes mission. *Space Science Reviews*, 179(1–4), 29–57. <https://doi.org/10.1007/s11214-012-9933-x>

Turner, D. L., Angelopoulos, V., Li, W., Hartinger, M. D., Usanova, M., Mann, I. R., et al. (2013). On the storm-time evolution of relativistic electron phase space density in Earth's outer radiation belt. *Journal of Geophysical Research: Space Physics*, 118, 2196–2212. <https://doi.org/10.1002/jgra.50151>

Turner, D. L., Morley, S. K., Miyoshi, Y., Ni, B., & Huang, C.-L. (2013). Outer radiation belt flux dropouts: Current understanding and unresolved questions. In D. Summers, I. R. Mann, D. N. Baker, & M. Schulz, (Eds.), *Dynamics of the Earth's radiation belts and inner magnetosphere, Geophysical Monograph Series*. Washington, DC: American Geophysical Union. <https://doi.org/10.1029/2012GM001310>

Tu, W., Selesnick, R., Li, X., &Looper, M. (2010). Quantification of the precipitation loss of radiation belt electrons observed by SAMPEX. *Journal of Geophysical Research: Space Physics*, 115. <https://doi.org/10.1029/2009ja014949>

van de Kamp, M., Rodger, C. J., Seppälä, A., Clilverd, M. A., & Verronen, P. T. (2018). An updated model providing long-term data sets of energetic electron precipitation, including zonal dependence. *Journal of Geophysical Research - D: Atmospheres*, 123, 9891–9915. <https://doi.org/10.1029/2017jd028253>

van de Kamp, M., Seppälä, A., Clilverd, M. A., Rodger, C. J., Verronen, P. T., & Whittaker, I. C. (2016). A model providing long-term data sets of energetic electron precipitation during geomagnetic storms. *Journal of Geophysical Research: Atmospheres*, 121(20), 2015JD024212. <https://doi.org/10.1002/2015jd024212>

Verronen, P. T., Andersson, M. E., Marsh, D. R., Kovács, T., & Plane, J. M. C. (2016). WACCM-D-Whole atmosphere community climate model with D-region ion chemistry. *Journal of Advances in Modeling Earth Systems*, 8, 954–975. <https://doi.org/10.1002/2015ms000592>

Verronen, P. T., Marsh, D. R., Szelag, M. E., & Kalakoski, N. (2020). Magnetic-local-time dependency of radiation belt electron precipitation: impact on ozone in the polar middle atmosphere. *Annales Geophysicae*, 38, 833–844. <https://doi.org/10.5194/angeo-38-833-2020>

Winningham, J. D., Sharber, J. R., Frahm, R. A., Burch, J. L., Eaker, N., Black, R. K., et al. (1993). The UARS particle environment monitor. *Journal of Geophysical Research*, 98(D6), 10649–10666. <https://doi.org/10.1029/93jd00461>

Yando, K., Millan, R. M., Green, J. C., & Evans, D. S. (2011). A Monte Carlo simulation of the NOAA POES medium energy proton and electron detector instrument. *Journal of Geophysical Research: Space Physics*, 116. <https://doi.org/10.1029/2011ja016671>